Title

The NKCC1 inhibitor bumetanide restores cortical feedforward inhibition and lessens sensory hypersensitivity in early postnatal fragile X mice.

Authors

Kourdougli, Nazim
Nomura, Toshihiro
Wu, Michelle
et al.

Publication Date

2024-06-01

DOI

10.1016/j.biopsych.2024.06.023

Journal Pre-proof

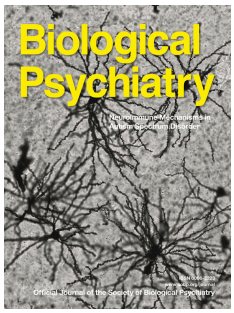

The NKCC1 inhibitor bumetanide restores cortical feedforward inhibition and lessens sensory hypersensitivity in early postnatal fragile X mice.

Nazim Kourdougli, Toshihiro Nomura, Michelle Wu, Anouk Heuvelmans, Zoë Dobler, Anis Contractor, Carlos Portera-Cailliau

PII: S0006-3223(24)01427-6

DOI: https://doi.org/10.1016/j.biopsych.2024.06.023

Reference: BPS 15531

To appear in: *Biological Psychiatry*

Received Date: 25 January 2024

Revised Date: 12 June 2024

Accepted Date: 25 June 2024

Please cite this article as: Kourdougli N., Nomura T., Wu M., Heuvelmans A., Dobler Z., Contractor A. & Portera-Cailliau C., The NKCC1 inhibitor bumetanide restores cortical feedforward inhibition and lessens sensory hypersensitivity in early postnatal fragile X mice., *Biological Psychiatry* (2024), doi: https://doi.org/10.1016/j.biopsych.2024.06.023.

The NKCC1 inhibitor bumetanide restores cortical feedforward inhibition and lessens sensory hypersensitivity in early postnatal fragile X mice.

Short title: Bumetanide lessens tactile defensiveness in Fragile X

Authors: Nazim Kourdougli[1], Toshihiro Nomura[2], Michelle Wu[1,3,4], Anouk Heuvelmans[1,¥], Zoë Dobler[1,3], Anis Contractor[2], and Carlos Portera-Cailliau[1,5,*]

Affiliations:

[1]Department of Neurology, University of California Los Angeles (UCLA)

[2]Department of Neuroscience, Northwestern University Feinberg School of Medicine

[3]Neuroscience interdepartmental graduate program, UCLA

[4]UCLA-Caltech Medical Scientist Training Program

[5]Department of Neurobiology, UCLA.

[¥] Current address: Erasmus MC, University of Rotterdam, Netherlands.

* Lead contact

Carlos Portera-Cailliau, MD, PhD

RNRC A-145

710 Westwood Plaza

Los Angeles, CA 90095

Email: cpcailliau@mednet.ucla.edu

Keywords: In vivo calcium imaging, Autism spectrum disorders, Intellectual disability, Fragile X syndrome, Interneuron, Bumetanide, NKCC1, Somatosensory cortex, Two-photon.

ABSTRACT:

Background: Exaggerated responses to sensory stimuli, a hallmark of Fragile X syndrome (FXS), contribute to anxiety and learning challenges. Sensory hypersensitivity is recapitulated in the *Fmr1* knockout (KO) mouse model of FXS. Recent studies in *Fmr1* KO mice have demonstrated differences in activity of cortical interneurons and a delayed switch in the polarity of GABA signaling during development. Previously, we reported that blocking the chloride transporter NKCC1 with the diuretic bumetanide, could rescue synaptic circuit phenotypes in primary somatosensory cortex (S1) of *Fmr1* KO mice. However, it remains unknown whether bumetanide can rescue earlier circuit phenotypes or sensory hypersensitivity in *Fmr1* KO mice.

Methods: We used acute and chronic systemic administration of bumetanide in *Fmr1* KO mice and performed in vivo 2-photon calcium imaging to record neuronal activity, while tracking mouse behavior with high-resolution videos.

Results: We demonstrate that layer (L) 2/3 pyramidal neurons in S1 of *Fmr1* KO mice show a higher frequency of synchronous events at postnatal day (P) 6 compared to wild-type controls. This was reversed by acute administration of bumetanide. Furthermore, chronic bumetanide treatment (P5-P14) restored S1 circuit differences in *Fmr1 KO* mice, including reduced neuronal adaptation to repetitive whisker stimulation, and ameliorated tactile defensiveness. Bumetanide treatment also rectified the reduced feedforward inhibition of L2/3 neurons in S1 and boosted the circuit participation of parvalbumin interneurons.

Conclusions: This further supports the notion that synaptic, circuit, and sensory behavioral phenotypes in *Fmr1* KO can be mitigated by inhibitors of NKCC1, such as the FDA-approved diuretic bumetanide.

INTRODUCTION

Atypical sensory processing is common in individuals with neurodevelopmental conditions (NDCs) and is one of the earliest symptoms in autistic toddlers (1). In Fragile X syndrome (FXS), the leading inherited form of intellectual disability and autism, hypersensitivity across multiple sensory domains is observed in most affected children (2,3), and leads to hyperarousal and maladaptive avoidance behaviors, such as tactile defensiveness (4,5). Sensory hypersensitivity exacerbates anxiety about social interactions and can contribute to inattention and learning disabilities (1). Therefore, identifying new treatments that alleviate sensory symptoms is of great value to FXS individuals, but also autistic people and those with other NDCs.

The excitation-inhibition (E-I) imbalance theory of autism (6) has been proposed as a common neural basis for many NDCs, including FXS (7,8). In the *Fmr1* knock-out (KO) mouse model of FXS, changes in E-I balance have been observed both at the synaptic and circuit levels(9–11), even during early developmental periods, although the changes are complex and cannot be explained by a simple unidimensional model of increased E-I ratio (12). We and others have demonstrated delays in the maturation of glutamatergic synapses as evidenced by persistently high turnover of dendritic spines of cortical pyramidal (Pyr) neurons during the first postnatal weeks (13–15) and their transient insensitivity to novel sensory experience (16). Moreover, *Fmr1* KO mice exhibit delays in the maturation of thalamocortical synaptic plasticity and the typical progressive decrease in synaptic NMDA/AMPA ratio and proportion of silent synapses during critical period development in S1 (17,18).

These changes in excitatory synapses and circuits in *Fmr1* KO mice occur in parallel with delays in the developmental sequence of GABAergic neurotransmission (19). For example, there is a reduction of excitatory inputs onto fast-spiking inhibitory interneurons (9,11) and their maturation in the neocortex is delayed (20). Moreover, the density of parvalbumin (PV)-expressing interneurons is reduced in the neocortex of *Fmr1* KO mice (21,22), presumably because they are hypoactive and decoupled from excitatory neurons (23). Finally, the depolarizing actions of the neurotransmitter GABA persists longer during development in *Fmr1* KO mice (24,25). This is due to a delay in the gradual change in the equilibrium potential for GABA (E_{GABA}) (26), which is governed by the shift in intracellular chloride concentration [Cl^-], the primary permeable ion through $GABA_A$ receptors. E_{GABA} is mediated by the function (27,28) and developmental expression of the neuronal-specific K^+-Cl^- extruder (KCC2) and the Na^+-K^+-$2Cl^-$ importer (NKCC1), which determine neuronal Cl^- homeostasis (29,30).

It is possible that prominent circuit phenotypes in *Fmr1* KO mice, including early network hypersynchrony (31–33), loss of neuronal adaptation to repetitive whisker stimulation (34) or changes in

E-I balance (10), could be caused by the delayed switch in GABA polarity, as suggested by recent studies (35–37). Recently, we showed that chronic systemic treatment of developing *Fmr1* KO mice with bumetanide, a blocker of the NKCC1 importer that rectifies Cl^- imbalance, could restore E_{GABA} in layer (L) 4 neurons of primary somatosensory cortex (S1), reverse synaptic delays in the development of thalamocortical inputs, and restore circuit plasticity during the critical period (17,38). However, important questions remain about the potential of bumetanide as a treatment for FXS. Can it restore the earliest circuit phenotypes in the neonatal brain of *Fmr1* KO mice, and can it alleviate sensory hypersensitivity at the behavior level?

Using in vivo 2-photon (2P) calcium imaging of L2/3 Pyr cells in S1, we demonstrate a higher frequency of synchronous events at postnatal day (P) 6 in *Fmr1* KO mice compared to wild-type (WT) controls. We also show that this neonatal network hyperactivity can be reversed by acute bumetanide administration at P6, and that chronic daily administration of bumetanide through critical period development (P5-P14) restores the synaptic E-I ratio by normalizing feedforward inhibition onto L2/3 neurons. Remarkably, the same chronic bumetanide treatment restored whisker-evoked circuit activity in S1 and lessened behavioral tactile defensiveness in P14-P16 *Fmr1* KO mice.

MATERIALS AND METHODS

Experimental animals:

All experiments followed the U.S. National Institutes of Health guidelines for animal research, under an animal use protocol (ARC #2007-035) approved by the Chancellor's Animal Research Committee and Office for Animal Research Oversight at the University of California, Los Angeles.

The following procedures are described in the Supplement: *Viral injections, Cranial windows, Intrinsic signal imaging, In vivo 2P calcium imaging in head-restrained mice, Intrinsic signal imaging, Drug administration, Tactile defensiveness assay in head-restrained mice, Brain slice electrophysiology and analysis, Data analysis for calcium imaging and Statistical analyses.*

RESULTS

Increased network activity in S1 barrel cortex of neonatal *Fmr1* KO mice

Previous studies have revealed that hypersynchrony of network activity in *Fmr1 KO* mice during the second postnatal week both in primary visual cortex and somatosensory cortex (23,31,33). There is also a higher firing rate of L2/3 Pyr neurons during Up-states in *Fmr1* KO mice at P14-P16, consistent with hyperexcitability (31,33). However, it is unclear when this difference in network excitability/synchrony is already present even earlier, during the first postnatal week. At least in vitro, excitatory neurons of *Fmr1* KO mice appear to be hyperexcitable as early as P0 in the hippocampus, or P4-5 in neocortex (24,32). We recently found that immature interneurons are hypoactive at P6 (23), but this could be a compensatory adjustment for Pyr cell hypoactivity (10).

Thus, we recorded network activity in vivo at P6 using 2P calcium imaging in unanesthetized WT and *Fmr1* KO mice expressing GCaMP6s (**Fig. 1A-B**). In both neonatal WT and *Fmr1* KO mice we observed intermittent synchronous network events of large amplitude and small spatial extent (**Fig. 1B-D**), consistent with the previously described 'patchwork' pattern of activity in the neonatal rodent brain (39–41). We found that both the frequency and amplitude of these synchronous network events at P6 were significantly higher in *Fmr1* KO mice compared to WT controls, by ~100% and 30%, respectively (**Fig. 1E-F**; p=0.027 for frequency and p=0.015 for amplitude). The mean correlation coefficients for neurons within 100 μm of each other were slightly higher in *Fmr1* KO mice (**Fig. 1G**; p=0.049; Student t-test), which is consistent with previous findings at ~P14 (31,33), although the mean for all pairs of neurons across the entire field of view were not different between genotypes at P6 (**Suppl. Fig 1**).

Reduced feedforward inhibition in L2/3 neurons of *Fmr1* KO mice is rescued by bumetanide.

Increased network excitability at P6 in *Fmr1* KO mice likely reflects an imbalance in the synaptic E-I ratio (10) due to lower GABAergic inhibition that is present in the first postnatal week (23) and persists into adulthood (10,42). Therefore, we assessed the function of the local microcircuit in L2/3 by recording the amplitude of monosynaptic EPSCs and di-synaptic IPSCs in L2/3 neurons in acute slices through the barrel cortex of juvenile mice (see *Supplementary Methods*). Whole-cell voltage clamp recordings were made, and the membrane potential was held at the reversal potential for either $GABA_A$ receptors or AMPA receptors. Under these recording conditions, IPSCs were reduced by ~80% in the presence of CNQX (10 μM; n= 5 cells, n= 5 mice; **Suppl. Fig. 2A-B**), suggesting that they are primarily mediated by di-synaptic

feedforward inhibition triggered by excitatory afferents from L4. IPSCs were fully blocked by the $GABA_A$ channel blocker picrotoxin (50 μM; **Suppl. Fig. 2C-D**).

We examined evoked L4→L2/3 EPSCs and IPSCs in slices from WT and *Fmr1* KO mice by stimulating L4 with incremental intensities of stimuli and recording synaptic responses in L2/3 neurons (**Fig. 2A**; see Supplementary *Methods*). We first compared WT and *Fmr1* KO mice that had received daily injections of chlorothiazide (CTZ; 10 mg/kg, i.p.), a control diuretic that does not cross the blood brain barrier (see below for rationale). There were no significant differences in the input-output (I-O) curves for EPSCs between recordings between *Fmr1* KO and WT mice (**Fig. 2B**; n= 19 and 16 cells in WT and *Fmr1* KO mice, respectively; $p = 0.98$). In contrast, and in agreement with a previous study (10), the I-O curves for IPSCs diverged significantly, as the amplitude of feedforward IPSCs was significantly reduced in *Fmr1* KO mice (**Fig. 2C**; Two-way ANOVA: $F_{(3, 62)} = 3.6$, $p < 0.0001$). Calculating the resulting E-I balance (see Supplementary *Methods*) demonstrated that the E-I ratio was significantly higher in *Fmr1* KO mice (**Fig. 2D**; Two-way ANOVA: $F_{(3, 62)} = 5.7$, $p < 0.0001$), again consistent with previous findings (10).

Previously, we discovered a delay in the maturation of E_{GABA} in L4 of S1 in *Fmr1* KO mice (25), and similar results have been reported for hippocampal neurons by another group (24). Notably, bumetanide, a loop-diuretic that lowers intracellular Cl^- levels through selective inhibition of the chloride importer NKCC1 at low doses (43,44), effectively dampens synchronous network activity (24,45,46). Subsequently, we demonstrated that chronic bumetanide treatment of *Fmr1* KO mice during the critical period rescues multiple synaptic and circuit phenotypes, including the enlarged size of whisker-evoked maps in S1 (38). However, it is not known whether the above-described changes in feedforward inhibition seen in L2/3 are also sensitive to pharmacological manipulation of E_{GABA}. Therefore, we tested whether chronic bumetanide treatment during the S1 critical period might restore L2/3 synaptic E-I balance in *Fmr1* KO mice.

We administered bumetanide (0.2 mg/kg, i.p.) or CTZ (10 mg.kg, i.p.) twice daily from P5 to P14 and then carried out in vitro electrophysiology after the closure of the cortical critical period when synaptic connections are stabilized (47) (**Fig. 2E**). Bumetanide has been proposed as a potential treatment for NDCs (48), but its effects could at least partially be mediated by diuresis rather than directly on NKCC1 in the brain (49). Thus, we compared bumetanide to CTZ, a thiazide diuretic that does not target NKCC1 and lacks brain permeability (50–52). We found that bumetanide treatment had no effect on the I-O curve for EPSCs in either WT or *Fmr1* KO mice (**Fig. 2F**; n= 16 and 15 cells, respectively; two-way ANOVA: $F_{(3, 62)} = 0.064$, $p= 0.98$). In contrast, chronic bumetanide treatment completely restored the I-O curves for IPSCs in *Fmr1* KO mice to WT levels (**Fig. 2G**; two-way ANOVA, $F_{(3, 62)} = 3.6$, $p > 0.99$). As a result, the change in

L2/3 synaptic E-I ratio observed in *Fmr1* KO mice was also not different to WT mice after bumetanide treatment (**Fig. 2H**; two-way ANOVA : $F_{(3, 62)} = 5.7$, $p > 0.99$).

Bumetanide reduces neuronal hyperexcitability in neonatal *Fmr1 KO* mice.

Based on these effects of bumetanide on E-I balance in vitro, and the fact that we had previously rescued thalamocortical synapse development in *Fmr1* KO mice at P10 and their enlarged whisker maps in S1 at P16-P17 with a similar chronic bumetanide treatment (38), we tested whether it could also rescue the increased frequency of synchronous network events during perinatal period at P6 (**Fig. 1**). We used in vivo 2P calcium imaging in WT and *Fmr1* KO mice at P6 to first record Pyr cell activity in L2/3 ~30 min after administering a single dose of CTZ (**Fig. 3A**). We found that the frequency of network events in WT mice that received CTZ was comparable to that in drug-naïve WT mice, suggesting that CTZ by itself does not affect the network (compare **Fig. 1E** and **Fig. 4B**). Next, after a 1 h rest period, we injected the same mice with bumetanide and recorded activity 30 min later (see Supplementary Methods). We found that bumetanide had no effect on the frequency of synchronous network events in WT mice compared to CTZ-treated controls (**Fig. 3B**; p=0.351; RM two-way ANOVA). However, bumetanide significantly reduced event frequency in *Fmr1* KO mice compared to CTZ treatment (**Fig. 3B**; p=0.015; RM two-way ANOVA). Pairwise correlation coefficients were slightly lower in both WT and *Fmr1* KO mice treated with bumetanide compared to their CTZ baseline, but the effect did not reach significance (**Fig. 3C**; p=0.113 for WT and p=0.142 for *Fmr1* KO; RM two-way ANOVA).

Taken together, these results show that not only is the S1 network of *Fmr1* KO mice hyperexcitable at P6, a time when PV interneuron precursors (but not somatostatin interneurons) are hypoactive (23) and a few days before network hyper-synchrony emerges (31,33), but also that it can be rescued by acute systemic bumetanide administration.

Chronic early postnatal treatment with bumetanide restores whisker responsiveness in S1 of *Fmr1 KO* mice.

We next asked whether chronic bumetanide treatment could also help restore whisker-responsiveness of Pyr cells in S1 to WT levels. We have previously shown that fewer L2/3 Pyr neurons in barrel cortex of *Fmr1* KO mice are whisker-responsive and that they show less adaptation with repetitive whisker stimulation (23,34). We performed in vivo 2P calcium imaging to record from L2/3 Pyr cells under light sedation at P15 following systemic treatment from P5 to P14 (twice daily) with either CTZ (10 mg/kg, i.p.) or bumetanide (0.2 mg/kg i.p.) in WT and *Fmr1* KO mice (**Fig. 4A**). Note that bumetanide

administration ended at least 20 h before calcium imaging, to avoid any acute effects of the drug. We recorded responses of L2/3 neurons to 20 sequential epochs of whisker stimulation at 10 Hz (1 s-long, every 3 s; see Supplementary Methods; **Fig. 4B**). Just as in our prior studies (34,53), we found that *Fmr1* KO mice (CTZ-treated) had a significantly lower percentage of whisker-responsive Pyr cells and showed significantly less adaptation to repetitive stimulation as compared to CTZ-treated WT controls (**Fig. 4C-D**; p=0.004 and p=0.001, respectively; two-way ANOVA, post hoc Bonferroni). Remarkably, *Fmr1* KO mice treated with bumetanide showed a significantly higher percentage of whisker-responsive cells and a higher adaptation index compared to CTZ-treated *Fmr1* KO mice (**Fig. 4C-D**; p=0.039 and p=0.047, respectively; two-way ANOVA, post hoc Bonferroni). This effect was specific to the FXS model mice because bumetanide had no effect on WT mice (**Fig. 4C-D**).

Chronic early postnatal bumetanide treatment ameliorates maladaptive tactile defensiveness in *Fmr1 KO* mice.

We previously reported that *Fmr1* KO mice show avoidance running and defensive behaviors to repetitive whisker stimulation, suggesting they perceived the stimulus as aversive (54). Such a maladaptive behavioral response to a sensory stimulus that is innocuous to WT mice is akin to tactile defensiveness in humans with FXS (2,3,55). Thus, we conducted experiments in *Fmr1* KO mice to determine the effect of chronic bumetanide treatment from P5 to P14 on tactile defensiveness at P15 (**Fig. 5A**). Head-fixed mice were allowed to run on a floating polystyrene ball treadmill while whiskers on one side of the snout were passively stimulated (see Supplementary *Methods*). Just as in our recent study (23), we observed that *Fmr1* KO mice treated with CTZ spent significantly more time showing defensive behaviors by grabbing the stimulator than WT-CTZ group (**Fig. 5B**; p=0.027; two-way ANOVA, post hoc Bonferroni). In contrast, *Fmr1* KO mice treated with bumetanide spent significantly less time grabbing the whisker stimulator than CTZ-treated *Fmr1* KO controls (**Fig. 5B**; p=0.018; two-way ANOVA, post hoc Bonferroni), showing levels of grabbing comparable to WT mice. Bumetanide treatment had no effect on WT mice. Using the same assay, we had previously reported that both WT and *Fmr1* KO mice increase their locomotion as an initial response to whisker stimulation; however, whereas WT mice habituate to the stimulation and show less running during the latter half of the protocol, *Fmr1* KO mice show persistent avoidance running throughout (34). Therefore, we quantified the amount of time that mice spent running at the end of the stimulation session for mice treated with bumetanide or CTZ. The total time spent running at the end of the stimulation was significantly higher in *Fmr1* KO-CTZ mice compared to WT-CTZ controls (**Fig. 5C**; p=0.026; two-way ANOVA, post hoc Bonferroni). *Fmr1* KO mice treated with bumetanide

spent significantly less time running than those treated with CTZ (**Fig. 5C**; p=0.078; two-way ANOVA, post hoc Bonferroni); in contrast, bumetanide treatment had no effect on WT mice. We did not observe any differences in the overall running time between genotypes or treatment groups during a control sham stimulation session in which the stimulator was placed beyond the reach of their whiskers (see Supplementary Methods) (**Suppl. Fig. 3**). In a subset of mice (n= 9 WT and 12 KO mice) that underwent both in vivo calcium imaging and behavior, we found that the degree of neuronal adaptation was strongly and significantly correlated with the degree of behavioral adaptation (decrease in avoidance running) (**Fig. 5D**). We conclude from these studies that chronic postnatal treatment with bumetanide significantly reduces tactile hypersensitivity in *Fmr1* KO mice.

Hypofunction of Parvalbumin-expressing interneurons (PV-INs) is a prominent phenotype in mouse models of autism (19). We and others have previously demonstrated that the activity of PV-INs is reduced in *Fmr1* KO mice and that a smaller proportion of them is active compared to WT mice in the developing S1 cortex (10,23,42). Additionally, we found that pharmacologically boosting PV-IN firing restored whisker-evoked activity in S1 and improved tactile defensiveness behaviors in *Fmr1* KO mice (10,23,42). Therefore, we wondered whether the beneficial effects we observed in *Fmr1* KO mice with bumetanide might be mediated, at least in part, through PV-INs. To this end, we chronically administered bumetanide (or CTZ) to *Fmr1* KO mice and then used *in vivo* two-photon calcium imaging at P15 in S1 to selectively monitor PV-IN activity using *Pvalb*-Cre$^{+/-}$ mice (**Fig 6A**). We found that PV-IN activity, as measured with the mean Z-scores of the magnitude of calcium transients, was unchanged after bumetanide treatment (**Fig 6B**, p=0.397 for spontaneous and p=0.281 for whisker-evoked activity, M-W test); however, the percentage of active PV-INs was significantly increased by chronic bumetanide treatment **(Fig 6C,** p=0.038 for spontaneous and p=0.049 for whisker-evoked activity, M-W- test). This suggests that bumetanide's effects on tactile defensiveness might not be directly mediated by chloride regulation in PV-INs but rather by how it affects their circuit engagement during sensory processing in *Fmr1* KO mice.

DISCUSSION

Here, we characterized the differences in excitatory S1 circuit dynamics in neonatal *Fmr1* KO mice and determined whether bumetanide could restore circuit function to WT levels and mitigate any sensory hypersensitivity. Our experiments reveal the following: 1) the frequency of synchronous network events of L2/3 Pyr neurons is significantly higher in *Fmr1* KO mice at P6 than in WT controls; 2) Chronic bumetanide treatment during the S1 critical period (P5-P14) restores feedforward inhibition in L2/3 in

Fmr1 KO mice; 3) Acute bumetanide injection in *Fmr1* KO mice restores this neonatal cortical hyperexcitability to WT levels; 4) Chronic bumetanide treatment of *Fmr1* KO mice also restores Pyr cell whisker-responsiveness and adaptation in S1 to WT levels, and alleviates behavioral tactile defensiveness. Thus, treatment with this FDA-approved diuretic during development improves a core sensory symptom in a model of FXS and could potentially have broader benefits in other NDCs.

Our study confirms and further extends several prior results on neuronal circuit differences in developing *Fmr1* KO mice. For example, similar to previous results (10,34,53), we demonstrate that whisker-responsiveness is reduced in Pyr cells in *Fmr1* KO mice and that they exhibit less adaptation than those in WT mice (Fig. 4). Similarly, just as we show at P6 (Fig. 1), an increased frequency of network events had already been shown for excitatory neurons in cortical slices from *Fmr1* KO mice at P4-P6 (32). Other studies had shown that cortical network activity is more synchronous in *Fmr1* KO mice than in WT controls after P8 (31,33), and our data suggest that such hypersynchrony is present as early as P6 (Fig. 1G). Note that we recently reported that, at P6, immature interneurons from the medial ganglionic eminence fire less in *Fmr1* KO mice than in WT controls (23), which suggests that interneuron hypoactivity is not a compensatory phenomenon but may instead be a primary driver of Pyr cell hyperactivity and hypersynchrony.

Our results also confirm previous findings that E-I ratio is increased in *Fmr1* KO mice due to a reduction in feedforward inhibition, though we did not observe the smaller parallel decrease in monosynaptic EPSCs that was also reported previously in *Fmr1* KO mice (10). This might be due to the fact that our recordings were performed in performed at a slightly older age (3-5 weeks vs. 2-3 weeks). However, overall our results agree with the finding that E-I ratio in L2/3 is elevated because of a change in feedforward inhibition and that delayed synaptic maturation in *Fmr1* KO mice eventually 'catch up' to WT levels as they reach adulthood.

Using *in vitro* electrophysiology in brain slices, we show that bumetanide treatment restores the E-I ratio in *Fmr1* KO mice by increasing feedforward inhibition to L2/3 of S1. These results build on those of our previous study showing that chronic bumetanide treatment corrects E_{GABA} and glutamatergic synapse formation in L4 neurons in *Fmr1* KO mice (38). While we have not determined the precise mechanism of how bumetanide affects synapses/circuits, our findings deepen our understanding about its impact on circuit development and further support its potential role in the treatment of NDCs. Although recent studies are beginning to assess the impact of bumetanide on the developmental trajectory of E_{GABA} in cortical interneurons (56,57), we do not yet know whether the delay of the E_{GABA} shift in *Fmr1* KO mice also affects interneurons. Because hypofunction of PV neurons is a prominent phenotype of *Fmr1* KO mice

(10,23,42), we tested the hypothesis that bumetanide's rescue of feedforward inhibition (Fig. 2) could be mediated through a direct increase of PV-IN activity. While chronic bumetanide treatment did not affect PV-IN firing rate, it did lead to an increase in the proportion of PV-INs that are engaged in the circuit (Fig. 6). A previous study had demonstrated that bumetanide does not contribute significantly to intracellular Cl^- regulation in PV-INs (57). Altogether, this suggests that as bumetanide shifts E_{GABA} towards more hyperpolarized membrane potentials in *Fmr1* KO mice, it thereby restores GABAergic inhibitory currents in *Fmr1* KO mice, rather than directly affecting PV-IN intrinsic firing.

It is worth mentioning that, while bumetanide regulates Cl^- homeostasis and subsequent neuronal activity both *in vivo* and *in vitro* through NKCC1 inhibition (48), bumetanide may have a widespread effect on gene regulation during development. Indeed, our previous proteomic analysis in developing *Fmr1* KO mice (18) revealed that several proteins responsible for proper integration of both glutamatergic and GABAergic circuit, such as PVALB and TrkB, were downregulated in *Fmr1* KO mice and could be upregulated after chronic bumetanide treatment. Interestingly, BDNF signaling through its tyrosine kinase receptor TrkB is associated with a maturation of PV interneurons (58). Hence, bumetanide treatment might restore delayed maturation of PV interneurons in *Fmr1* KO mice via TrkB signaling.

Bumetanide is an FDA-approved diuretic and holds promise for the treatment for NDCs (48). However, some have questioned whether its effects in rodents are due to NKCC1 inhibition in the brain because of its poor central nervous system bioavailability (49), though others have documented brain penetrability in neonates (59,60). Moreover, its diuretic effects are believed to limit its beneficial use for treating NDCs (60–62). To control for this, we compared bumetanide to another effective diuretic (CTZ) that does not target NKCC1 and KCC2 and does not cross the blood brain barrier (50–52). In our study, we showed that in *Fmr1* KO mice, bumetanide, but not CTZ, restored E-I balance, reduced neonatal network excitability in vivo and lessened sensory deficits, in ways that CTZ could not, consistent with prior studies (38,63). Genetic downregulation of NKCC1 also results in lower neuronal excitability (46,64), further confirming the potential therapeutic effect of NKCC1 blockade in NDCs. Of note, higher NKCC1 protein levels have been reported in several rodent models of NDCs including FXS (24,25) as well as in humans with Down Syndrome (48).

Despite the disappointing results of two recent Phase 3 clinical trials of bumetanide in sporadic autism (65), the results of our preclinical studies in *Fmr1* KO mice add to other evidence supporting the use of NKCC1 inhibitors in single-gene NDCs like FXS (66).

Acknowledgments: The authors thank Anand Suresh for ideas and suggestions throughout the project and John Armstrong for help with bumetanide injections. This work was supported by the following grants: R01NS117597 (NIH-NINDS) and R01HD054453 (NIH-NICHD) awarded to C.P.-C., Department of Defense (DOD, 13196175) awarded to C.P-C and A.C., R01HD108370 (NIH-NICHD) awarded to C.P-C and A.C., a grant from the FRAXA foundation awarded to N.K., Madeline Julie Vervoort Fund (Amsterdam University, #7682) to A.H, and the T32 UCLA-Caltech MSTP to M.W. No preprint version of this manuscript was made available on Biorxiv prior to publication in *Biological Psychiatry*.

Conflict of Interests: The authors report no biomedical financial interests or potential conflicts of interest.

REFERENCES

1. Robertson CE, Baron-Cohen S (2017): Sensory perception in autism. *Nature Reviews Neuroscience* 18: 671–684.

2. Miller LJ, McIntosh DN, McGrath J, Shyu V, Lampe M, Taylor AK, *et al.* (1999): Electrodermal responses to sensory stimuli in individuals with fragile X syndrome: A preliminary report. *Am J Méd Genet* 83: 268–279.

3. Molen MJWV der, Molen MWV der, Ridderinkhof KR, Hamel BCJ, Curfs LMG, Ramakers GJA (2012): Auditory and visual cortical activity during selective attention in fragile X syndrome: A cascade of processing deficiencies. *Clin Neurophysiol* 123: 720–729.

4. Baranek GT, Foster LG, Berkson G (1997): Tactile defensiveness and stereotyped behaviors. *Am J Occup Ther* 51: 91–95.

5. Rais M, Binder DK, Razak KA, Ethell IM (2018): Sensory Processing Phenotypes in Fragile X Syndrome. *ASN NEURO* 10: 1759091418801092.

6. Rubenstein JLR, Merzenich MM (2003): Model of autism: increased ratio of excitation/inhibition in key neural systems. *Genes Brain Behav* 2: 255–267.

7. Nomura T (2021): Interneuron Dysfunction and Inhibitory Deficits in Autism and Fragile X Syndrome. *Cells* 10: 2610.

8. Contractor A, Klyachko VA, Portera-Cailliau C (2015): Altered Neuronal and Circuit Excitability in Fragile X Syndrome. *Neuron* 87: 699–715.

9. Domanski APF, Booker SA, Wyllie DJA, Isaac JTR, Kind PC (2019): Cellular and synaptic phenotypes lead to disrupted information processing in Fmr1-KO mouse layer 4 barrel cortex. *Nature Communications* 10: 4814–18.

10. Antoine MW, Langberg T, Schnepel P, Feldman DE (2019): Increased Excitation-Inhibition Ratio Stabilizes Synapse and Circuit Excitability in Four Autism Mouse Models. *Neuron* 101: 648-661.e4.

11. Gibson JR, Bartley AF, Hays SA, Huber KM (2008): Imbalance of neocortical excitation and inhibition and altered UP states reflect network hyperexcitability in the mouse model of fragile X syndrome. *Journal of Neurophysiology* 100: 2615–2626.

12. O'Donnell C, Gonçalves JT, Portera-Cailliau C, Sejnowski TJ (2017): Beyond excitation/inhibition imbalance in multidimensional models of neural circuit changes in brain disorders. *bioRxiv* 086363.

13. Cruz-Martín A, Crespo M, Portera-Cailliau C (2010): Delayed stabilization of dendritic spines in fragile X mice. *Journal of Neuroscience* 30: 7793–7803.

14. Pan F, Aldridge GM, Greenough WT, Gan W-B (2010): Dendritic spine instability and insensitivity to modulation by sensory experience in a mouse model of fragile X syndrome. *Proc Natl Acad Sci* 107: 17768–17773.

15. Padmashri R, Reiner BC, Suresh A, Spartz E, Dunaevsky A (2013): Altered Structural and Functional Synaptic Plasticity with Motor Skill Learning in a Mouse Model of Fragile X Syndrome. *J Neurosci* 33: 19715–19723.

16. Arroyo ED, Fiole D, Mantri SS, Huang C, Portera-Cailliau C (2019): Dendritic Spines in Early Postnatal Fragile X Mice Are Insensitive to Novel Sensory Experience. *Journal of Neuroscience* 39: 412–419.

17. Harlow EG, Till SM, Russell TA, Wijetunge LS, Kind P, Contractor A (2010): Critical Period Plasticity Is Disrupted in the Barrel Cortex of Fmr1 Knockout Mice. *Neuron* 65: 385–398.

18. He Q, Arroyo ED, Smukowski SN, Xu J, Piochon C, Savas JN (2018): Critical period inhibition of NKCC1 rectifies synapse plasticity in the somatosensory cortex and restores adult tactile response maps in fragile X mice. *Mol Psychiatry* 8: 109–16.

19. Contractor A, Ethell IM, Portera-Cailliau C (2021): Cortical interneurons in autism. *Nat Neurosci* 24: 1648–1659.

20. Nomura T, Musial TF, Marshall JJ, Zhu Y, Remmers CL, Xu J, *et al.* (2017): Delayed Maturation of Fast-Spiking Interneurons Is Rectified by Activation of the TrkB Receptor in the Mouse Model of Fragile X Syndrome. *J Neurosci* 37: 11298–11310.

21. Selby L, Zhang C, Sun Q-Q (2007): Major defects in neocortical GABAergic inhibitory circuits in mice lacking the fragile X mental retardation protein. *Neuroscience Letters* 412: 227–232.

22. Wen TH, Afroz S, Reinhard SM, Palacios AR, Tapia K, Binder DK, *et al.* (2018): Genetic Reduction of Matrix Metalloproteinase-9 Promotes Formation of Perineuronal Nets Around Parvalbumin-Expressing Interneurons and Normalizes Auditory Cortex Responses in Developing Fmr1 Knock-Out Mice. *Cereb Cortex* 28: 3951–3964.

23. Kourdougli N, Suresh A, Liu B, Juarez P, Lin A, Chung DT, *et al.* (2023): Improvement of sensory deficits in fragile X mice by increasing cortical interneuron activity after the critical period. *Neuron* 111: 2863-2880.e6.

24. Tyzio R, Nardou R, Ferrari DC, Tsintsadze T, Shahrokhi A, Eftekhari S, *et al.* (2014): Oxytocin-mediated GABA inhibition during delivery attenuates autism pathogenesis in rodent offspring. *Science* 343: 675–679.

25. He Q, Nomura T, Xu J, Contractor A (2014): The Developmental Switch in GABA Polarity Is Delayed in Fragile X Mice. *Journal of Neuroscience* 34: 446–450.

26. Ben-Ari Y, Khalilov I, Kahle KT, Cherubini E (2012): The GABA Excitatory/Inhibitory Shift in Brain Maturation and Neurological Disorders. *neuroscientist* 18: 467–486.

27. Hübner CA, Lorke DE, Hermans-Borgmeyer I (2001): Expression of the Na-K-2Cl-cotransporter NKCC1 during mouse development. *Mech Dev* 102: 267–269.

28. Yamada J, Okabe A, Toyoda H, Kilb W, Luhmann HJ, Fukuda A (2004): Cl− uptake promoting depolarizing GABA actions in immature rat neocortical neurones is mediated by NKCC1. *J Physiol* 557: 829–841.

29. Rivera C, Voipio J, Payne JA, Ruusuvuori E, Lahtinen H, Lamsa K, *et al.* (1999): The K+/Cl− co-transporter KCC2 renders GABA hyperpolarizing during neuronal maturation. *Nature* 397: 251–255.

30. Kurki SN, Uvarov P, Pospelov AS, Trontti K, Hübner AK, Srinivasan R, *et al.* (2022): Expression patterns of NKCC1 in neurons and non-neuronal cells during cortico-hippocampal development. *Cereb Cortex*.

31. Gonçalves JT, Anstey JE, Golshani P, Portera-Cailliau C (2013): Circuit level defects in the developing neocortex of Fragile X mice. *Nat Neurosci* 16: 903–909.

32. La Fata GL, Gärtner A, Domínguez-Iturza N, Dresselaers T, Dawitz J, Poorthuis RB, *et al.* (2014): FMRP regulates multipolar to bipolar transition affecting neuronal migration and cortical circuitry. 17: 1693–1700.

33. Cheyne JE, Zabouri N, Baddeley D, Lohmann C (2019): Spontaneous Activity Patterns Are Altered in the Developing Visual Cortex of the Fmr1 Knockout Mouse. *Front Neural Circuits* 13: 57.

34. He CX, Cantu DA, Mantri SS, Zeiger WA, Goel A, Portera-Cailliau C (2017): Tactile Defensiveness and Impaired Adaptation of Neuronal Activity in the Fmr1 Knock-Out Mouse Model of Autism. *J Neurosci : Off J Soc Neurosci* 37: 6475–6487.

35. Flossmann T, Kaas T, Rahmati V, Kiebel SJ, Witte OW, Holthoff K, Kirmse K (2019): Somatostatin Interneurons Promote Neuronal Synchrony in the Neonatal Hippocampus. *Cell Rep* 26: 3173-3182.e5.

36. Kirmse K, Zhang C (2022): Principles of GABAergic signaling in developing cortical network dynamics. *Cell Rep* 38: 110568.

37. Murata Y, Colonnese MT (2020): GABAergic interneurons excite neonatal hippocampus in vivo. *Sci Adv* 6: eaba1430.

38. He Q, Arroyo ED, Smukowski SN, Xu J, Piochon C, Savas JN, *et al.* (2019): Critical period inhibition of NKCC1 rectifies synapse plasticity in the somatosensory cortex and restores adult tactile response maps in fragile X mice. *Mol Psychiatry* 24: 1732–1747.

39. Babij R, Ferrer C, Donatelle A, Wacks S, Buch AM, Niemeyer JE, *et al.* (2023): Gabrb3 is required for the functional integration of pyramidal neuron subtypes in the somatosensory cortex. *Neuron* 111: 256-274.e10.

40. Siegel F, Heimel JA, Peters J, Lohmann C (2012): Peripheral and central inputs shape network dynamics in the developing visual cortex in vivo. *Curr Biol* 22: 253–258.

41. Golshani P, Gonçalves TJ, Khoshkoo S, Mostany R, Smirnakis S, POrtera-Cailliau C. (2009) Internally Mediated Developmental Desynchronization of Neocortical Network Activity. J Neurosci 29:10890–10899.

42. Goel A, Cantu DA, Guilfoyle J, Chaudhari GR, Newadkar A, Todisco B, *et al.* (2018): Impaired perceptual learning in a mouse model of Fragile X syndrome is mediated by parvalbumin neuron dysfunction and is reversible. *Nat Neurosci* 21: 1–14.

43. Sato SS, Artoni P, Landi S, Cozzolino O, Parra R, Pracucci E, *et al.* (2017): Simultaneous two-photon imaging of intracellular chloride concentration and pH in mouse pyramidal neurons in vivo. *Proc Natl Acad Sci* 114: E8770–E8779.

44. Gamba G, Miyanoshita A, Lombardi M, Lytton J, Lee WS, Hediger MA, Hebert SC (1994): Molecular cloning, primary structure, and characterization of two members of the mammalian electroneutral sodium-(potassium)-chloride cotransporter family expressed in kidney. *J Biol Chem* 269: 17713–17722.

45. Kirmse K, Kummer M, Kovalchuk Y, Garaschuk O, Holthoff K (2015): GABA depolarizes immature neurons and inhibits network activity in the neonatal neocortex in vivo. *Nature Communications* 6: 7750.

46. Graf J, Zhang C, Marguet SL, Herrmann T, Flossmann T, Hinsch R, *et al.* (2021): A limited role of NKCC1 in telencephalic glutamatergic neurons for developing hippocampal network dynamics and behavior. *Proc Natl Acad Sci* 118: e2014784118.

47. Wen JA, Barth AL (2011): Input-specific critical periods for experience-dependent plasticity in layer 2/3 pyramidal neurons. *J Neurosci : Off J Soc Neurosci* 31: 4456–65.

48. Ben-Ari Y (2017): NKCC1 Chloride Importer Antagonists Attenuate Many Neurological and Psychiatric Disorders. *Trends Neurosci* 40: 536–554.

49. Löscher W, Kaila K (2022): CNS pharmacology of NKCC1 inhibitors. *Neuropharmacology* 205: 108910.

50. Doniger S, Hofmann T, Yeh J (2002): Predicting CNS permeability of drug molecules: comparison of neural network and support vector machine algorithms. *J Comput Biol* 9: 849–864.

51. Gamba G, Miyanoshita A, Lombardi M, Lytton J, Lee WS, Hediger MA, Hebert SC (2001): Molecular cloning, primary structure, and characterization of two members of the mammalian electroneutral sodium-(potassium)-chloride cotransporter family expressed in kidney. *J Biological Chem* 269: 17713–17722.

52. Sivakumaran S, Maguire J (2015): Bumetanide reduces seizure progression and the development of pharmacoresistant status epilepticus. *Epilepsia* 57: 222–232.

53. Kourdougli N, Suresh A, Liu B, Juarez P, Lin A, Chung DT, *et al.* (2023): Improvement of sensory deficits in fragile X mice by increasing cortical interneuron activity after the critical period. *Neuron*. Sep 20;111(18):2863-2880.e6.

54. He CX, Cantu DA, Mantri SS, Zeiger WA, Goel A (2017): Tactile Defensiveness and Impaired Adaptation of Neuronal Activity in the Fmr1Knock-Out Mouse Model of Autism. *J Neurosci* 37: 6475–6487.

55. Butler MG, Mangrum T, Gupta R, Singh DN (1991): A 15-item checklist for screening mentally retarded males for the fragile X syndrome. *Clin Genet* 39: 347–354.

56. Skorput AG, Lee SM, Yeh PW, Yeh HH (2019): The NKCC1 antagonist bumetanide mitigates interneuronopathy associated with ethanol exposure in utero. *eLife* 8: e48648.

57. Otsu Y, Donneger F, Schwartz EJ, Poncer JC (2020): Cation–chloride cotransporters and the polarity of GABA signalling in mouse hippocampal parvalbumin interneurons. *J Physiol* 598: 1865–1880.

58. Huang ZJ, Kirkwood A, Pizzorusso T, Porciatti V, Morales B, Bear MF, *et al.* (1999): BDNF regulates the maturation of inhibition and the critical period of plasticity in mouse visual cortex. *Cell* 98: 739–755.

59. Cleary RT, Sun H, Huynh T, Manning SM, Li Y, Rotenberg A, *et al.* (2013): Bumetanide Enhances Phenobarbital Efficacy in a Rat Model of Hypoxic Neonatal Seizures ((M. Avoli, editor)). *PLoS ONE* 8: e57148.

60. Delpire E, Ben-Ari Y (2022): A Wholistic View of How Bumetanide Attenuates Autism Spectrum Disorders. *Cells* 11: 2419.

61. Römermann K, Fedrowitz M, Hampel P, Kaczmarek E, Töllner K, Erker T, *et al.* (2017): Multiple blood-brain barrier transport mechanisms limit bumetanide accumulation, and therapeutic potential, in the mammalian brain. *Neuropharmacology* 117: 182–194.

62. Savardi A, Borgogno M, Vivo MD, Cancedda L (2021): Pharmacological tools to target NKCC1 in brain disorders. *Trends Pharmacol Sci* 42: 1009–1034.

63. Deidda G, Parrini M, Naskar S, Bozarth IF, Contestabile A, Cancedda L (2015): Reversing excitatory GABAAR signaling restores synaptic plasticity and memory in a mouse model of Down syndrome. *Nat Med* 21: 318–326.

64. Parrini M, Naskar S, Alberti M, Colombi I, Morelli G, Rocchi A, *et al.* (2021): Restoring neuronal chloride homeostasis with anti-NKCC1 gene therapy rescues cognitive deficits in a mouse model of Down syndrome. *Mol Ther* 29: 3072–3092.

65. Ben-Ari Y, Cherubini E (2022): The GABA Polarity Shift and Bumetanide Treatment: Making Sense Requires Unbiased and Undogmatic Analysis. *Cells* 11: 396.

66. Lemonnier E, Robin G, Degrez C, Tyzio R, Grandgeorge M, Ben-Ari Y (2013): Treating Fragile X syndrome with the diuretic bumetanide: a case report. 102: e288–e290.

FIGURE LEGENDS

Figure 1: Higher frequency of Pyr cell network activity in S1 of *Fmr1* KO mice at P6.

A. Experimental design for in vivo calcium imaging at P6 in WT and *Fmr1* KO mice. P1 mice are injected with AAV11-Syn-GCaMP6s and recorded at P6.
B. Left: Example field of view of L2/3 Pyr cells expressing GCaMP6s in S1 cortex at P6. Right: Same field of view showing different clusters of synchronous network events at different times during the recording session. Scale bar 100 µm.
C. Representative traces of Pyr cells calcium transients in WT and *Fmr1* KO mice.
D. Raster plots of Pyr cell activity in representative WT and *Fmr1* KO mice. Note the higher event frequency in *Fmr1 KO*.
E. The frequency of synchronous network events for Pyr cells was significantly higher in *Fmr1* KO mice (0.9 ± 0.2 for WT vs. 1. 8 ± 0.3 for *Fmr1 KO* mice; p= 0.027, n=8 WT and n=9 *Fmr1* KO mice, Kolmogorov-Smirnov test). The filled-in symbols in panels E-G correspond to the same animals from which traces and rasters shown in panels C & D.
F. The amplitude of network events for Pyr cells was significantly higher in *Fmr1 KO* mice compared to WT controls (24.3 ± 2.5 for WT vs. 31.1 ± 1.4 for; *Fmr1* KO mice; n=8 WT and n=9 *Fmr1* KO mice p= 0.015, Kolmogorov-Smirnov test).
G. Mean correlation coefficient for all cell pairs within 100 µm in WT and *Fmr1* KO mice. (0.74 ± 0.03 in 8 WT mice vs. 0.82 ± 0.029 in *Fmr1* KO mice; n=8 WT and n=9 *Fmr1* KO mice; p=0.049, unpaired t test).

Figure 2: Reduced feedforward inhibition in L2/3 in *Fmr1* KO mice is rescued by chronic developmental treatment with bumetanide.

A. Cartoon representation of the microcircuit in the S1 cortex and the recording configuration. L4 principal neurons send excitatory projections onto both interneurons and pyramidal neurons in L2/3. Activated L2/3 interneurons send feedforward inhibitory projections onto pyramidal neurons. Monosynaptic EPSCs and di-synaptic IPSCs (feedforward inhibition) were recorded from L2/3 pyramidal neurons.

B. Representative traces of L4-evoked EPSC and disynaptic IPSC recorded in L2/3 at reversal potentials of IPSCs (-50 mV) and EPSCs (0 mV) in in 3-5 weeks old WT and *Fmr1*$^{-/-}$ mice treated with either chlorothiazide (CTZ) or bumetanide (Bumet). Calibration: 50 ms, 500 pA.

C. I-O curves of EPSCs following incremental stimulation steps of 20 µA in WT and *Fmr1* KO mice treated with CTZ. No difference were observed between genotypes (n=19 cells from 9 WT-CTZ mice and n=16 cells from 8 *Fmr1* KO-CTZ mice; two-way ANOVA: $F_{(3, 62)} = 0.064$, $p = 0.98$). Plots in panels C-H show the mean ± SEM.

D. I-O curves of IPSCs following incremental stimulation steps of 20 µA in WT and *Fmr1* KO mice treated with CTZ. IPSCs are significantly reduced in *Fmr1* KO mice (n=19 cells from 9 WT-CTZ mice and n=16 cells from 8 *Fmr1* KO-CTZ mice two-way ANOVA, $F_{(3, 62)} = 3.6$, $p > 0.99$).

E. E-I conductance ratio calculated as E/(E+I) is higher in *Fmr1* KO-CTZ compared to WT-CTZ mice (n= 16 from 6 WT-CTZ mice and n=15 cells from 7 *Fmr1* KO-CTZ mice).

F. I-O curves of EPSCs following incremental stimulation steps of 20 µA in WT and *Fmr1* KO mice treated with bumetanide. No differences were observed between treated groups (n=16 cells from 6 WT mice and: n=15 cells from 7 *Fmr1* KO mice; two-way ANOVA, p= 0.98).

G. I-O curves of IPSCs following incremental stimulation steps of 20 µA in WT and *Fmr1* KO mice treated with Bumet. Note the rescue of bumetanide treatment on the IPSCs in *Fmr1* KO mice (n=16 cells from 6 WT mice and: n=15 cells from 7 *Fmr1* KO mice; two-way ANOVA).

H. E-I conductance ratio calculated as E/(E+I) is not different in *Fmr1* KO bumet treated mice compared to WT bumet treated mice. (WT: n= 16 and *Fmr1* KO mice: n=15 cells; two-way ANOVA, $p > 0.99$).

Figure 3: Acute bumetanide administration reduces the frequency of synchronous network events at P6 in *Fmr1* KO mice.

A. Experimental design for in vivo calcium imaging at P6 in WT and *Fmr1* KO mice treated first with chlorothiazide (CTZ) and then, 80-120min later with bumetanide (Bumet). Mice were injected with AAV11-Syn-GCaMP6S at P1 and recorded at P6.

B. The frequency of synchronous network events for Pyr cells in *Fmr1* KO mice was significantly reduced upon acute bumetanide treatment (1.6 ± 0.2 events.min^{-1} for *Fmr1* KO-CTZ vs. 1.1±0.2 events.min^{-1} for *Fmr1* KO-Bumet, p=0.015; RM two-way ANOVA, post hoc Bonferroni), but it had no effect in WT mice (1.2±0.1 events.min^{-1} for WT-CTZ vs. 1.3±0.2 events.min^{-1} for WT-Bumet, p=0.351; RM two-way ANOVA, post hoc Bonferroni). n=7 mice per group, females are represented by circles and males by squares.

C. Pairwise correlation coefficients of Pyr cells were unchanged by acute bumetanide treatment in both WT and *Fmr1* KO mice (0.44±0.04 for WT -CTZ vs. 0.34±0.05 for WT-Bumet, p=0.113; 0.49±0.04 for *Fmr1* KO-CTZ vs. 0.33±0.16 for *Fmr1* KO-Bumet, p=0.142; RM two-way ANOVA, post hoc Bonferroni).

Figure 4: Chronic postnatal bumetanide treatment rescues whisker-evoked S1 circuit activity in *Fmr1* KO mice at P15.

A. Experimental design for in vivo calcium imaging in WT and *Fmr1* KO mice at P15 following chronic treatment with either CTZ (10 mg/kg) or Bumet (0.2 mg/kg). Twice daily i.p. injections from P5 to P14.

B. Whisker-evoked calcium traces of five example L2/3 Pyr cells from a *Fmr1* KO mouse.

D. The percentage of whisker-responsive Pyr cells was significantly lower in *Fmr1 KO*-CTZ mice than in WT-CTZ controls, but bumetanide treatment reversed this (WT-CTZ: 40.7±2.5%, WT-Bumet: 37.5 ± 3.5%, *Fmr1* KO-CTZ: 22.6±3.3%, *Fmr1* KO-Bumet: 36.0±4.5%; two-way ANOVA, post hoc Bonferroni, n=10 WT and n=12 *Fmr1* KO mice, respectively). Note that Bumet treatment did not change the whisker-responsiveness of WT mice. Female mice are represented by circles and males by squares.

C. The adaptation index of Pyr cells was significantly lower in *Fmr1* KO-CTZ mice compared to WT-CTZ controls, but bumetanide treatment partially reversed this (WT-CTZ: 0.28±0.09, WT-Bumet: 0.29±0.3, *Fmr1* KO-CTZ: -0.04±0.04, *Fmr1* KO-Bumet: 0.15±0.04). Note that bumetanide treatment did not change the Pyr cell adaptation in WT mice.

Figure 5: Chronic postnatal treatment of *Fmr1* KO mice with bumetanide ameliorates their maladaptive tactile defensiveness at P15.

A. Top: Experimental design for in vivo calcium imaging at P15 following chronic treatment with CTZ or Bumet (twice daily from P5 to P14) in WT and *Fmr1* KO mice. Bottom: Cartoon of tactile defensiveness behavioral assay. Head-fixed mice receive 20 bouts of whisker stimulation while we monitor with cameras their behavioral responses.

B. The proportion of time spent grabbing the stimulator (defensive behavior) was significantly higher in *Fmr1 KO*-CTZ mice than in WT-CTZ controls, but bumetanide rescued this phenotype (WT-CTZ: 6.0±2.9%, n=11; WT-Bumet: 5.8±1.7%, n= 14; *Fmr1* KO-CTZ: 21.2±3.9%, n=15; *Fmr1* KO-Bumet: 6.5±3.7%, n=13; two-way ANOVA, post hoc Bonferroni). Female mice are represented by circles, and males by squares.

C. Time spent running during the last 5 bouts of whisker stimulation was significantly higher in *Fmr1* KO-CTZ compared to WT-CTZ controls, and Bumet rescued this phenotype (WT-CTZ: 2.9±1.3 s; WT-Bumet: 2.9±1.4s; *Fmr1* KO -CTZ: 10.2±1.9s; *Fmr1* KO-Bumet: 4.1±2.1%; two-way ANOVA, post hoc Bonferroni).

D. Behavioral adaptation plotted against the neuronal adaptation indices to repetitive whisker-stimulation, with Spearman's correlations. (WT-CTZ: r=0.779, *p*=0.017, n=9; WT-Bumet: r=0.774, *p*=0.026, n= 9; *Fmr1* KO-CTZ: r 0.659, *p*= 0.0142, n=12; *Fmr1 KO*-Bumet: r=0.762, *p*=0.023, n=12). Note that only a subset of the mice underwent both 2P calcium imaging and tactile defensiveness behavioral assay.

Figure 6: Chronic administration of bumetanide from P5 to P14 increases the proportion of active PV-INs at P15 in *Fmr1* KO mice.

A. Cartoon of experimental design. *PValb-Cre;Fmr1* KO mice were injected with a Cre-dependent GCaMP6s virus allowing for specific targeting of calcium imaging in PV-INs.

B. Mean Z-scores of PV-INs during spontaneous and whisker-evoked activity at P15 in *Fmr1* KO mice after bumetanide or CTZ treatment. (spontaneous: 1.59±0.29 for CTZ vs. 1.77±0.17 for bumetanide; p=0.397, M-W t-test; whisker-evoked: 2.33±0.33 for CTZ vs. 1.83±0.29 for bumetanide; p=0.281, M-W t-test, n=7 *Fmr1* KO-CTZ and n=8 *Fmr1* KO-Bumet mice). Female mice are represented by circles and males by squares.

C. Percentage of active PV-INs after chronic bumetanide or CTZ treatment (spontaneous: 79.3±0.1% for CTZ vs. 96.6±0.0% for for bumetanide; p=0.038 , M-W t-test, n=28 fov for CTZ and n=37 FOV for bumetanide; whisker-evoked: 82.5±0.1% for CTZ vs. 97.4±0.0% for bumetanide; p=0.049, M-W t-test).

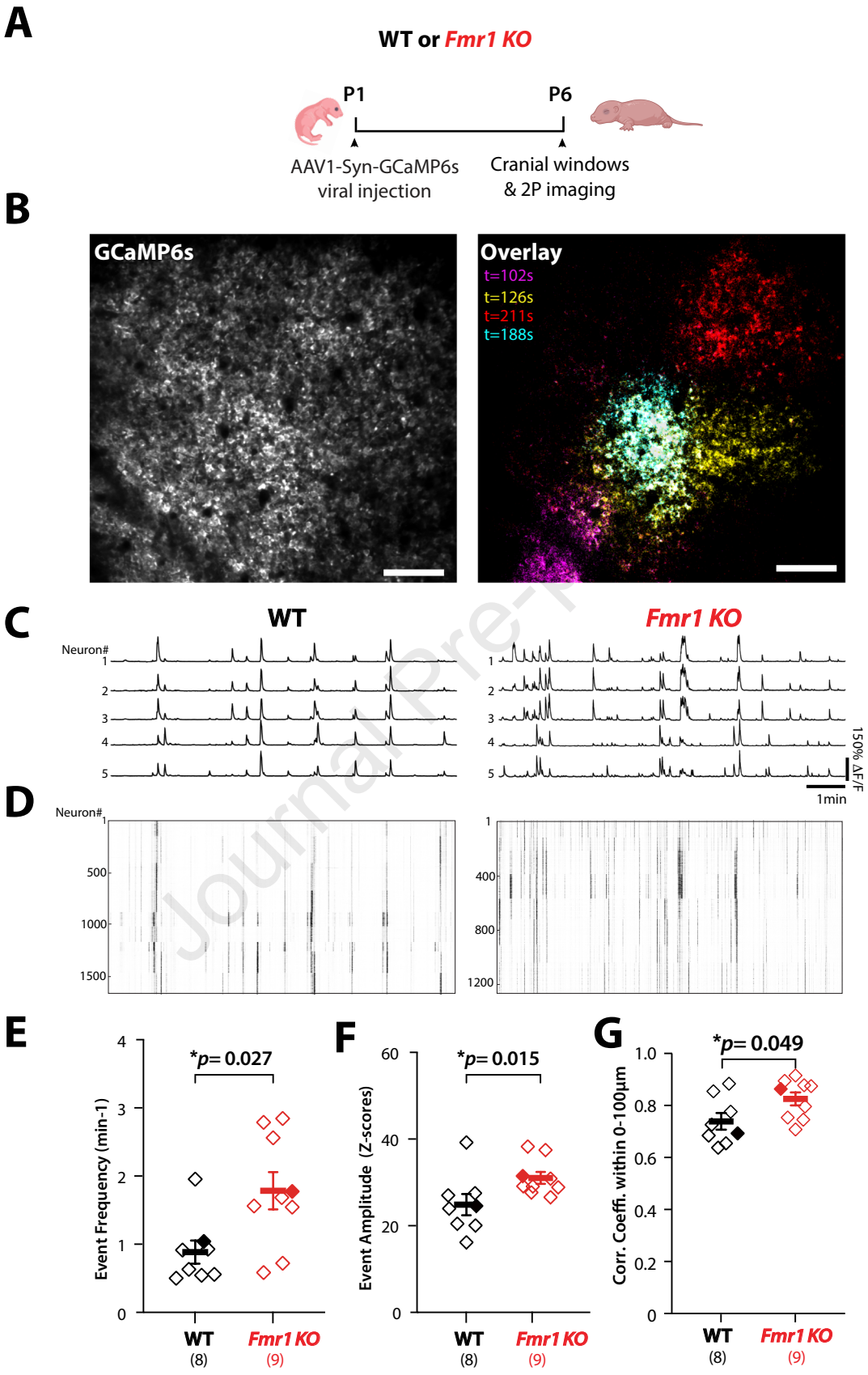

FIGURE 1

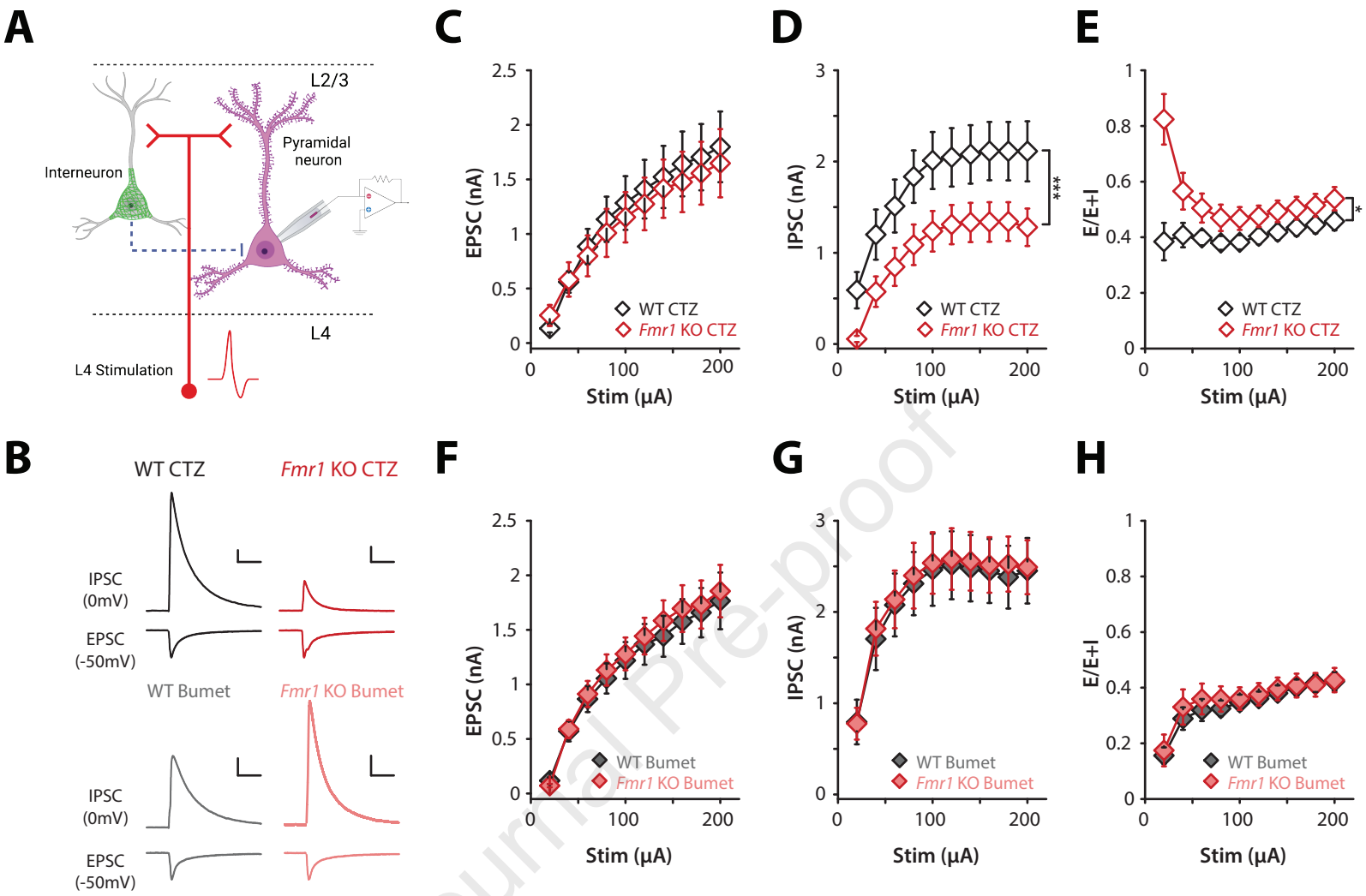

FIGURE 2

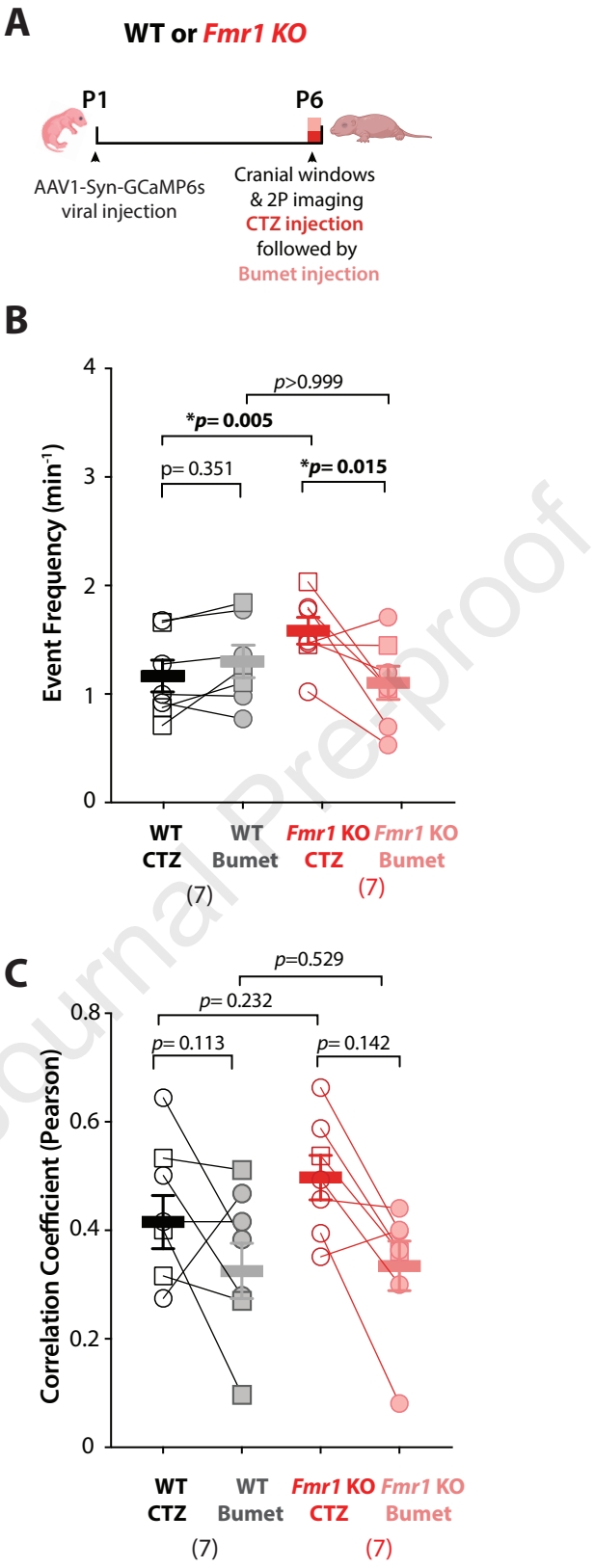

FIGURE 3

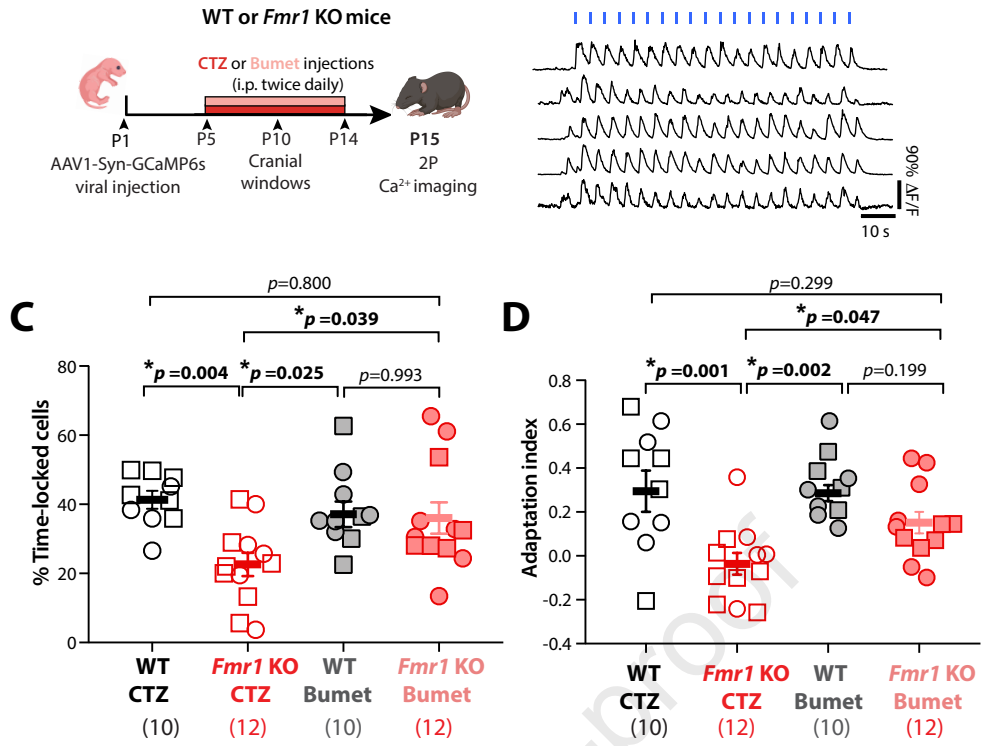

FIGURE 4

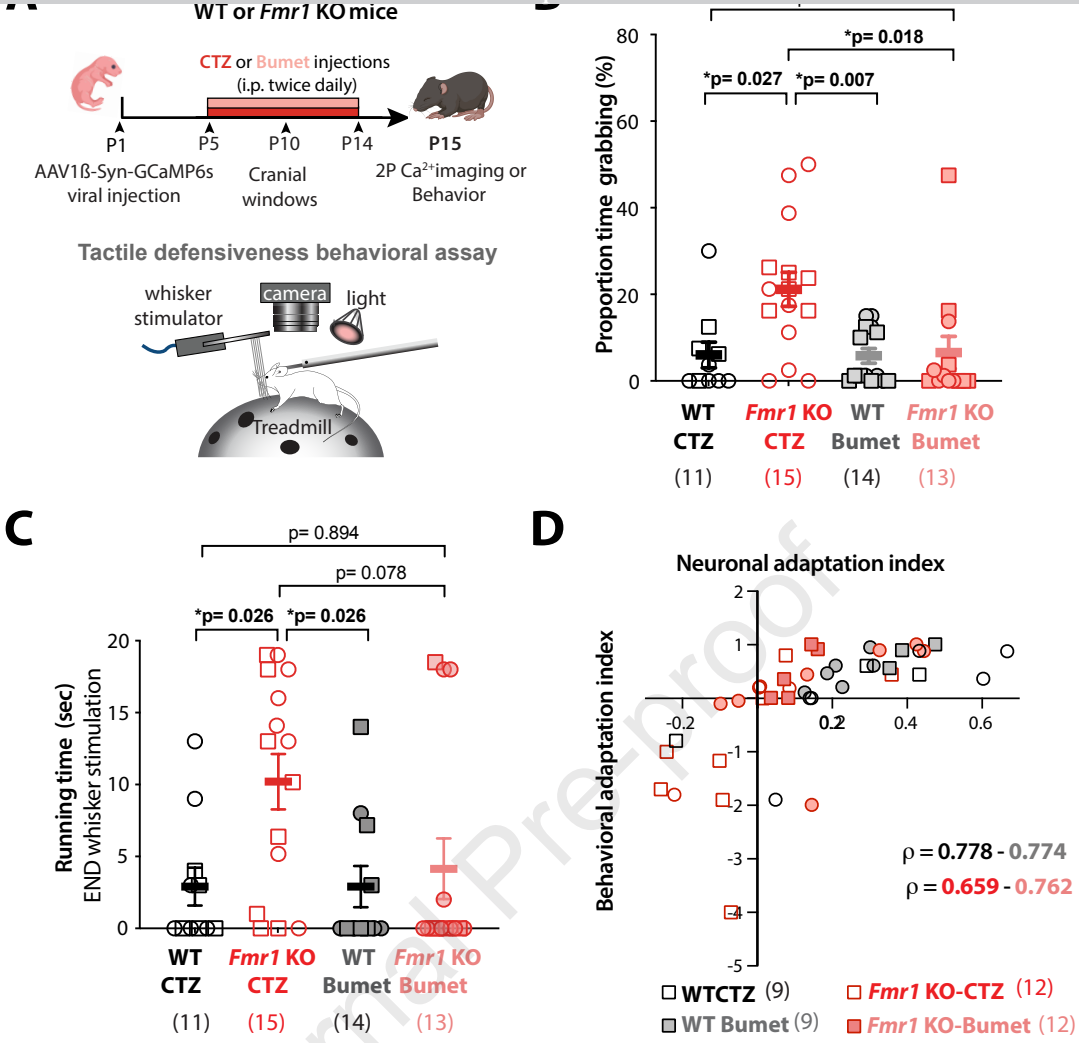

FIGURE 5

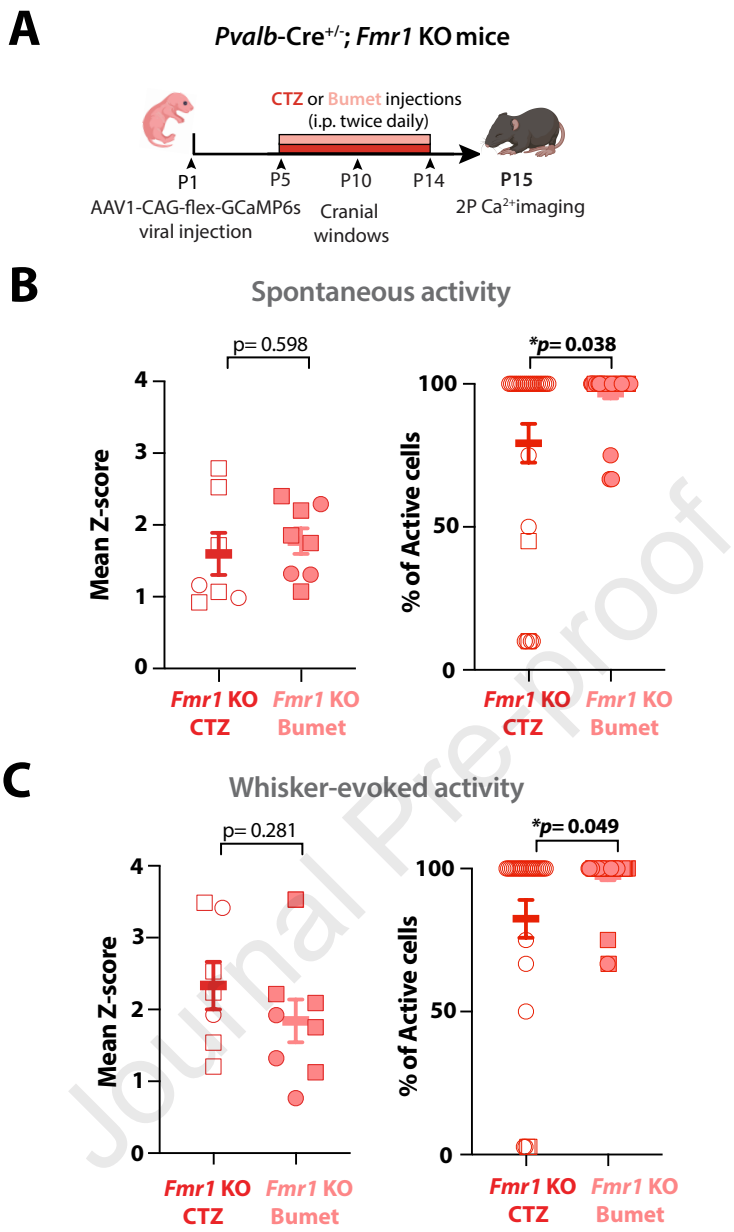

FIGURE 6